

# Properties of force networks in jammed granular media

Xiaoliang Deng<sup>1</sup> · Rajesh N. Davé<sup>1</sup>

Received: 10 November 2016 / Published online: 18 March 2017  
© Springer-Verlag Berlin Heidelberg 2017

**Abstract** Discrete element method simulations are conducted to investigate the effects of applied uniaxial compressive load, and bidisperse particle size distributions on force networks within jammed granular media. The differences between the strong and weak networks are examined through investigating the spatial correlation and distribution of contact angles, and emergence of chainlike structures. The simulation results show that the chainlike structures are more prevalent in the strong network due to the larger cumulative probabilities of contact angles, but not all the contacts belonging to the strong or weak networks are able to constitute the chainlike structures. Although the contacts of coarse-fine particles are dominant for the bidisperse systems, the contacts of coarse-coarse particles dominate the strong network, as well as the linear chainlike structures. Upon increasing the pressure from very low to high, the probability of contact orientations with respect to the compression direction in the strong network increases for contact orientation less than  $60^\circ$  and decreases for contact orientation greater than  $60^\circ$ , while the opposite trends are observed in the weak network. The tails of normalized normal contact forces distributions are quantified by  $P(f) = \exp(-cf^n)$ , and it is found that the value of  $n$  depends on the applied pressure and particle size distribution. Statistical analysis shows that the degree of homogeneity of contact force increases with increasing pressure, which is also validated by participation number.

**Keywords** DEM simulation · Contact force · Jamming · Force chain

✉ Rajesh N. Davé  
dave@njit.edu

<sup>1</sup> New Jersey Center for Engineered Particulates, New Jersey Institute of Technology, Newark, NJ 07102, USA

## 1 Introduction

Jamming occurs when a system develops a yield stress in a disordered state [1]. When subjected to the external force, the jammed granular media develops heterogeneous force networks to transmit stress at the boundaries through the interparticle contacts [2–4]. Such force networks are the key to understanding various phenomena associated with granular materials, such as jamming transition, and mechanical properties of static and dynamic dense granular media [5–13]. According to the magnitudes of contact forces, it is known from earlier studies that force networks in jammed granular media can be further decomposed into two categories: strong contact network and weak contact network, corresponding to the contacts carrying the forces larger or smaller than the mean contact force, respectively [14–16]. The nonsliding strong contacts form chainlike structures and carry the majority of the loading and the weak network behaves essentially like an interstitial liquid [14]. The percolation of such strong network in all directions signals a fully sheared jammed state [17]. However, to date, there is no general theory about spontaneous emergence of such chainlike structures.

In terms of quantitative analysis of the interparticle contact forces, they are usually characterized by the probability distribution function (PDF)  $P(f)$ , defined as the probability for finding a contact force with a specific magnitude. Experimental results demonstrate that the contact force distribution is a signature of jamming transition [5]. In spite of intense recent research on the particle packing under confined stress, identification of the characteristic of tail of contact force distribution remains one of the long-standing fundamental problems in granular physics. Early experimental measurements using carbon paper technique [18–20] and contact dynamics simulations [21] or discrete element method [22–

[24] reported that the PDF decays exponentially for the normal forces larger than the mean normal contact force. However, faster than exponential decay is also observed in the later experiments using photoelastic particles, emulsions, and liquid droplets [2, 5, 25], supported by numerical simulations [6, 8, 26, 27]. Along with the experiments, many attempts have also been made to explain the tail behavior of PDF, such as  $q$  model [28] and statistical description [29], supporting exponential and Gaussian tail, respectively. Furthermore, there is no consensus with regard to the distribution for the contact forces smaller than the mean. For example,  $q$  model predicts the PDF approaches zero when contact force approaches zero [28], which is inconsistent with experimental data [20]. In addition, using contact dynamics approach, the statistical distribution for normal and tangential contact forces lower than mean value decays with power law, however, the statistical distribution for contact forces higher than mean values decays exponentially [21], indicating the statistical model probably applies only to the strong force network [21]. The discrepancy among the model predictions and available experimental data indicates that further research is required in order to provide improved understanding of the behavior of jammed granular media. A promising and feasible way to test robustness of various theories is to investigate the jamming under various conditions such as different loads, and particle size distributions.

In this paper, DEM simulations are designed to investigate the effects of various applied uniaxial compressive loads and bidisperse particle size on force networks within jammed granular media. Of specific interest is to unravel the difference between the strong and weak networks by investigating the spatial correlation and distribution of contact angle, chainlike structures in the strong and weak networks, and the response to external loads, which are distinct from previous work that addressed the complementary mechanical properties of strong and weak force networks [14, 30]. By probing the linear chainlike structures in the strong and weak networks within jammed particles with monodisperse and bidisperse size distributions, it is found that not all the contacts in the strong and weak networks are able to form the chainlike structure. Further, the chainlike structure is more prevalent in the strong network, which can be explained by the cumulative probabilities of contact angles. In addition, it is also found that the contact orientations in the strong and weak networks exhibit the opposite responses to the compressive loads. For bidisperse system, the various types of contacts are analyzed for strong, weak, and chainlike force networks as well. Finally, the probability distribution of contact force as a function of pressure has been examined as well.

The DEM simulation and the methods employed to generate the jammed configurations are introduced in Sect. 2. The results and discussions regarding contact force networks, var-

ious types of contacts in the bidisperse systems, response of contact orientation to the external loads, and statistical distribution of contact force are presented in Sect. 3, followed by conclusions in Sect. 4.

## 2 Simulation approach

A DEM approach is used to simulate particle packing between two parallel plates composed of particles on the top and bottom of the packing. The initial configurations are obtained by randomly placing particles within simulation domain without any overlap between any two. The particles settle down at the bottom plate under the gravity and a gradually increasing compressive force in the negative  $z$  direction is exerted on the top plate until it reaches a prescribed value. Total 3200 glued particles with same material properties constituted the top and bottom plates [31]. The periodic boundary conditions are employed in both  $x$  and  $y$  directions to eliminate the side wall effect. At each simulation step, the total forces exerted by the bulk particles on the top plate are computed and then equally assigned to all the particles belonging to the top plate so that all of them move together. Meanwhile, the bottom plate keeps still during the simulations. Thereafter, pressure, which is the ratio of compressive force to the area of top plate, is used to quantify the degree of compression. Compressive loadings ranged from very low to high, namely, 0.001, 0.01, 0.1, 1, 10 and 100 MPa.

The interparticle interactions are described via nonlinear elastic Hertz–Mindlin spring–dashpot model where the dissipative damping forces are proportional to the relative normal and tangential velocities [32, 33]. The tangential force is additionally subject to the Coulomb friction threshold. The governing equations for individual particles can be written as follows,

$$m_i \frac{d\vec{v}_i}{dt} = \sum_{j \neq i}^k \vec{F}_{ij} + m_i \vec{g} \quad (1)$$

$$I_i \frac{d\vec{\omega}_i}{dt} = \sum_{j \neq i}^k \vec{T}_{ij} \quad (2)$$

$$\vec{F}_{ij} = \vec{F}_{ij}^n + \vec{F}_{ij}^t \quad (3)$$

$$\vec{T}_{ij} = \vec{R}_i \times \vec{F}_{ij}^t - \vec{\tau}_{ij}^r \quad (4)$$

where  $m_i$ ,  $\vec{v}_i$ ,  $\vec{\omega}_i$ ,  $\vec{R}_i$ ,  $I_i$  represent the mass, translational velocity, rotational velocity, vector connecting the center of particle  $i$  and the contact point, and the moment of inertia of particle  $i$ .  $\vec{F}_{ij}$  is the contact force induced by particle  $j$  and it can be divided into two parts: normal contact force  $\vec{F}_{ij}^n$  and tangential contact force  $\vec{F}_{ij}^t$ .  $\vec{T}_{ij}$  represents the torque induced by particle  $j$  due to tangential contact force and

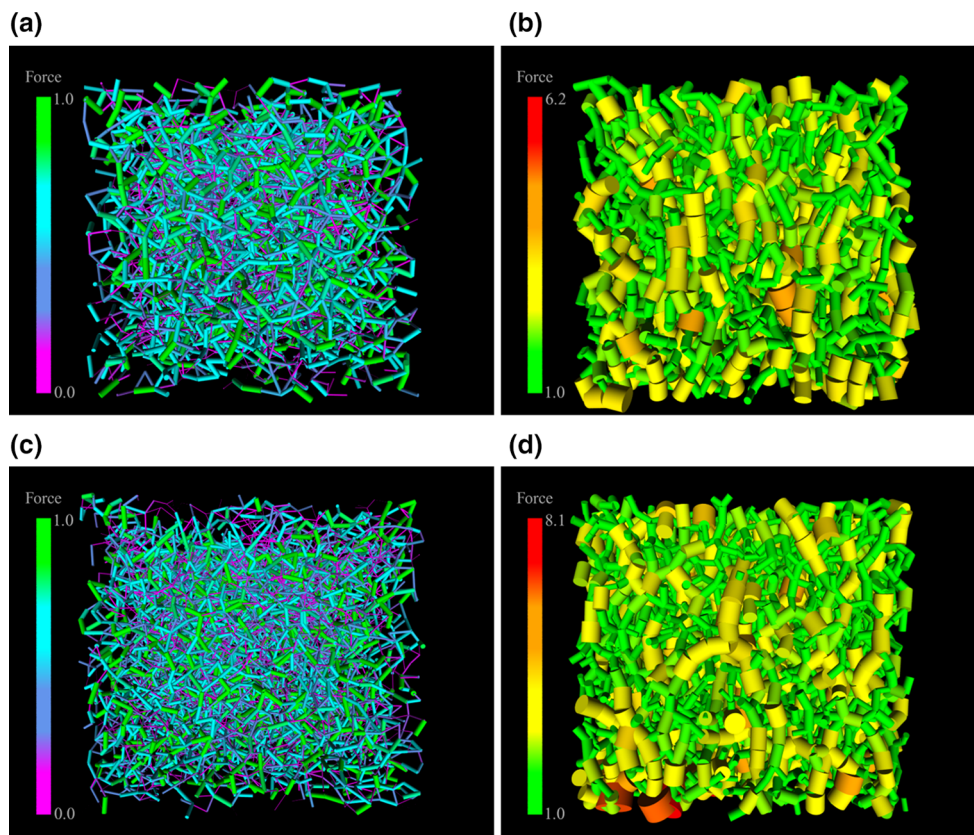


**Fig. 1** Weak and strong force networks for the monodisperse and bidisperse systems at the pressure of 100MPa. Contact vectors are shown using a cylinder connecting the centers of two contacting particles, where the diameter and color (violet–red) of the cylinders indicate the

magnitude of corresponding contact forces (*low–high*). **a, b** Weak and strong force networks for monodisperse system. **c, d** Weak and strong force networks for bidisperse system (color figure online)

rolling friction force ( $\vec{\tau}_{ij}^r$ ). The total contact force and torque are the summation over the  $k$  particles contacting with particle  $i$ . Further details about contact models can be found in the references [34,35].

The packing simulations with monodisperse as well as bidisperse size distribution are carried out. The monodisperse simulation systems consist of total 5000 particles with diameter of 1.0mm. The bidisperse simulation systems consist of 4000 large particles with diameter of 1.0mm and 4629 smaller particles with diameter of 0.6mm (mass ratio of smaller particles to the total mass of particles is equal to 0.2). The microscopic parameters defining particle properties are, the shear modulus of 29 Gpa, the Poisson ratio of 0.2, the friction coefficient of 0.3, and the density of  $2.0 \times 10^3 \text{ kg/m}^3$ .

### 3 Results and discussion

#### 3.1 Contact force networks

Based on the magnitude of force carried by a contact, the contact network can be further divided into the weak and

strong networks [14, 15]. The contacts involved in the strong network carry the force larger than a cutoff force and vice versa in the weak network. In this paper, the cutoff force is set to be the mean of all contacts [14]. The strong and weak contact networks for monodisperse and bidisperse systems at the highest pressure of 100MPa are depicted in Fig. 1. Contact vectors are shown using a cylinder connecting the centers of two contacting particles and the diameter and color (violet to red) of cylinders indicate the magnitude of corresponding contact forces (low to high). It can be seen that for both the monodisperse and bidisperse systems, the contact segments in the strong network spatially prefer to form a chainlike structure along the compressive direction (vertical). Those observations are consistent with experimental results using frictionless droplets [25].

Various methods have been applied to characterize the chainlike structure of contact network in the literature [36–39]. In this study, in order to quantitatively analyze the chainlike structure in both weak and strong contact networks, two angles  $\theta_1$  and  $\theta_2$  between three adjoining contact force segments are defined in Fig. 2 [38]. This is illustrated for particle 1 in Fig. 2 to determine if it is in a chainlike structure

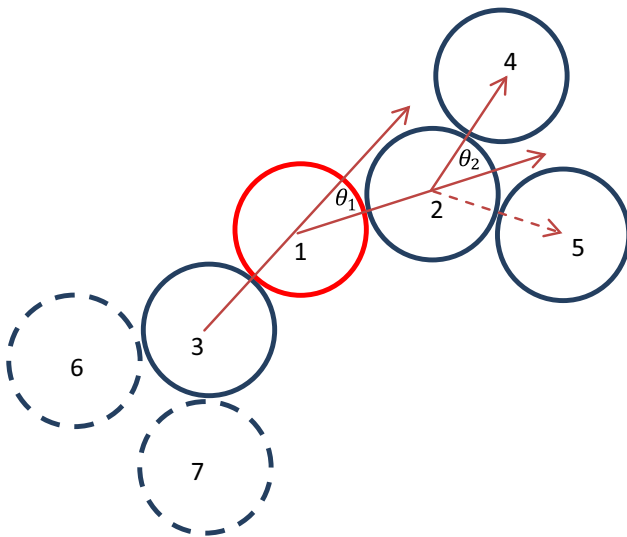


**Fig. 2** A schematic of chainlike structure analysis

or not. First, its two neighboring particles with two largest contact forces are chosen (particles 2 and 3). Next, all the neighboring particles of particle 2 are determined, which are shown as particle 4 and 5. It should be noted that in this step only those neighboring particles with contact forces greater than mean value are counted for strong contact network, in contrast, only those neighboring particles with contact forces less than mean value are counted for weak contact network. Once the neighbors in the chain are identified, the value of angles  $\theta_1$  and  $\theta_2$  can be computed. The similar process is followed for particle 3, which is another neighboring particle of particle 1. The force chain is allowed to have a reasonable degree of curvature [37], therefore, particles 3, 1, 2, and 4 are regarded as linear chainlike arrangements as long as both  $\theta_1$  and  $\theta_2$  are less than  $45^\circ$  (tolerance angle). Compared with other methods that characterized the force chains [38,40], the method presented here is able to identify the branching or emerging chainlike structures. Here, the minimum number of particles involved into chainlike structure is four, instead of two or three [37,39,41]. As will be discussed later, the effect of the tolerance angle value on the overall trends is also examined.

Figure 3 presents the extracted chainlike structures using the method described above in both the weak and strong contact networks. For the chainlike structures in the strong network, they preferentially arrange themselves along the compressive direction for both monodisperse and bidisperse systems. The longest chainlike structure in Fig. 3b is composed of 13 individual particles. Whereas, there are 12 large particles plus 3 small particles constituting the longest chainlike structure in Fig. 3d. More importantly, there are no preferential arrangements along compressive direction for the chainlike structures in the weak network, and the longest network length is shorter than that in the strong network.

As evident, the stress state in this investigation is anisotropic due to uniaxial compression. For the monodisperse size distribution, the three principle stresses of stress tensor along x, y, and z axis are  $\sigma_{xx} = 0.00045$  MPa,  $\sigma_{yy} = 0.00046$  MPa,  $\sigma_{zz} = 0.00064$  MPa for the compressive loading of 0.001 MPa and  $\sigma_{xx} = 35.5$  MPa,  $\sigma_{yy} = 34.6$  MPa,  $\sigma_{zz} = 58.5$  MPa for the compressive loading of 100 MPa. For the bidisperse size distribution (mass ratio of smaller particles to the total mass of particles is equal to 0.2), the three principle stresses of stress tensor along x, y, and z axis are  $\sigma_{xx} = 0.00046$  MPa,  $\sigma_{yy} = 0.00045$  MPa,  $\sigma_{zz} = 0.00064$  MPa for the compressive loading of 0.001 MPa and  $\sigma_{xx} = 34.0$  MPa,  $\sigma_{yy} = 33.4$  MPa,  $\sigma_{zz} = 57.3$  MPa for the compressive loading of 100 MPa (the compressive direction is along z direction in both cases). The focus of this study is the properties of contact force networks under uniaxial compression. However, the method of applying external loading should be another important factor influencing properties of contact force network but beyond the scope of the current work. In addition, gravitational force can enhance interparticle interaction along z direction, thus leading to the anisotropy of stress tensor. However, the influence of gravitational force is expected to be minor at high compressive pressure.

Figure 4a displays the fraction of chainlike contacts as a function of pressure in the strong and weak networks for monodisperse and bidisperse systems. It can be observed that about 60% of contacts in the strong network are able to form chainlike structures for both systems, almost independent of the pressures. Interestingly, however, for both monodisperse and bidisperse systems about 32% of contacts in the weak network evolve into the chainlike structures at the lowest pressure of 0.001 MPa, and the percentage increases to about 45% at the highest pressure of 100 MPa. This dependence on the pressure for the case of weak networks indicates that they can reorganize and form more chainlike structures upon increasing pressure in order to effectively augment the stability of strong networks at higher pressures. Therefore, the chainlike structures in the strong and weak networks exhibit different responses to the external compressive pressures. Another observation is that not all contacts in the strong network are able to constitute the chainlike structures, which qualitatively agrees with the previous 2D DEM simulation results [37]. It is emphasized that the chainlike structures in the weak network are explored for the first time in this study. Interestingly, the results indicate that the same is also true for the weak networks, where even less than half of the contacts evolve into the chainlike structure. Overall, the chainlike structure is more prevalent in the strong networks compared to the weak networks.

The fraction of contacts involved in strong networks with respect to the total contacts is also illustrated in Fig. 4b. The results show that the strong contacts for bidisperse systems



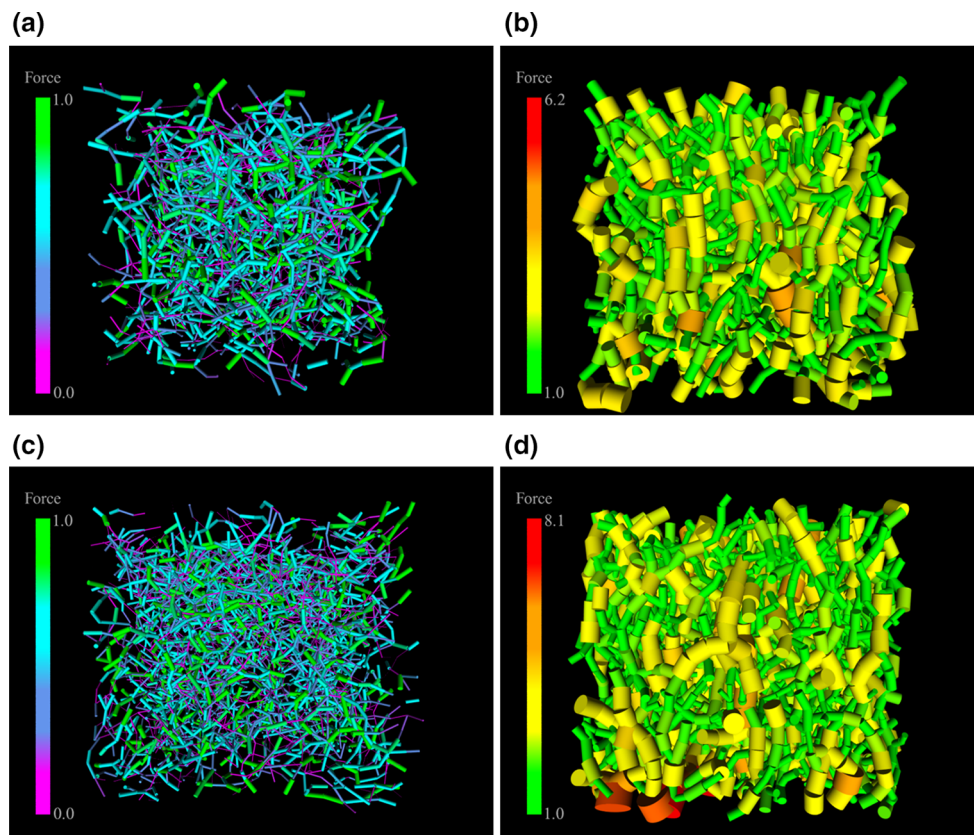


**Fig. 3** Linear chainlike structures for the monodisperse and bidisperse systems at the pressure of 100 MPa. Contact vectors are shown using a cylinder connecting the centers of two contacting particles and the diameter and color (violet–red) of cylinders indicate the magnitude of

corresponding contact forces (*low–high*). **a, b** Weak and strong force networks for monodisperse system. **c, d** Weak and strong force networks for bidisperse system (color figure online)

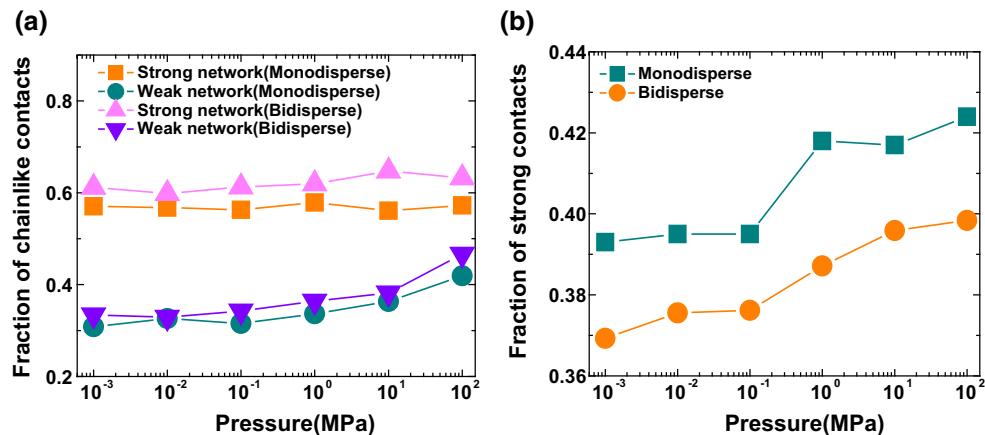


**Fig. 4 a** Fraction of chainlike contacts in the strong and weak networks as a function of pressure for monodisperse and bidisperse systems. **b** Fraction of strong contacts with respect to the total contacts as a function of pressure

consist of about 37–40% of total contacts, slightly increasing with the pressures. This part of the result is in agreement with previous 2D contact dynamic simulations [14]. For the monodisperse system, the fraction of contacts in the strong force network with respect to the total number of contacts

is about 39–42%, which is comparable with the bidisperse system.

For identifying the chainlike structure, tolerance angle as an artificial parameter is required in the algorithm. In order to ensure that the conclusions are independent of the

specific values of tolerance angle, a sensitivity analysis is performed. The tolerance values are changed from minimum  $10^\circ$  to maximum  $45^\circ$  and the results indicate that although the fraction of chainlike structures in both strong and weak networks decreases with decreasing tolerance value as expected, the fraction of chainlike structures in the strong network is always larger than that of the weak network, indicating the conclusion is robust with respect to the choice of the tolerance angle.

Assuming that the contact forces tend to form a linear chain structure, the correlations in the orientation of neighboring contacts, represented by  $\theta_1$  and  $\theta_2$ , are expected. To further understand the emergence of the chainlike structures, the Pearson correlation coefficient  $R = cov(\theta_1, \theta_2) / (\sigma_{\theta_1} \sigma_{\theta_2})$ , where  $cov(\theta_1, \theta_2)$  is the covariance of  $\theta_1$  and  $\theta_2$ , and  $\sigma_{\theta_1}, \sigma_{\theta_2}$  are the standard deviations of  $\theta_1$  and  $\theta_2$ , is computed to quantify the correlation between  $\theta_1$  and  $\theta_2$ . The results indicate that the Pearson correlation coefficients are negative. For monodisperse and bidisperse systems, the minimum values are about  $-0.04$  and  $-0.07$  for strong and weak chainlike structures, respectively, indicating no correlation in either strong or weak chainlike structures. The previous experimental results using quasi-two dimensional emulsions show that there is no correlation in the strong chainlike structure [38]. Our results are in good agreement with this conclusion.

To further explore the tendency for strong and weak networks to form the linear chainlike structures, the distribution of  $\theta_1$  and  $\theta_2$  is analyzed. A similar method has been applied in the literature [38]. During the process of statistical analysis, both  $\theta_1$  and  $\theta_2$  are treated as a single variable  $\theta$ . Figure 5 shows the cumulative probabilities of  $\theta$  at the lowest and highest pressures for monodisperse and bidisperse systems. The distributions indicate that the probabilities for  $\theta < 45^\circ$  in the strong network are slightly higher than that of in the weak network, regardless of the pressure and particle size

distributions. Therefore, compared with the contacts in the weak network, the contacts in the strong network arrange themselves in such a way that relative angles between them are more likely to be smaller than  $45^\circ$ , which explains the higher prevalence of linear chainlike structures in the strong network.

### 3.2 Various types of contacts in bidisperse system

For bidisperse system, the contact network can be categorized not only depending on the magnitude of contact forces, but also the size of particles in contact, including the contacts constituted by coarse-coarse (CC), coarse-fine (CF), and fine-fine (FF) particles. The corresponding fractions of those specific types of contacts with respect to the total number of contacts are shown in Fig. 6a as a function of compression pressure. It can be seen that the fractions of CF contacts are roughly 50% with respect to the total number of contacts and the contacts in bidisperse system are therefore dominated by CF contacts in our simulations. Similarly, Fig. 6b shows the fractions of specific type of contacts in the strong contact network as a function of pressure. Surprisingly, although about 50% contacts with respect to the total contacts are CF contacts, 60% contacts in the strong contact network are CC contacts. In other words, the CF contacts dominate the total contact network but CC contacts dominate the strong contact network.

Since not all the contacts in the strong network form linear chainlike structure, the fractions of specific contacts in chainlike structures are also examined and the results are shown in Fig. 6c. It can be seen that CC contacts dominate the chainlike structures as well. Figure 6d shows the fraction of chainlike contacts in the weak contact network as a function of pressure, indicating that the dominating type of

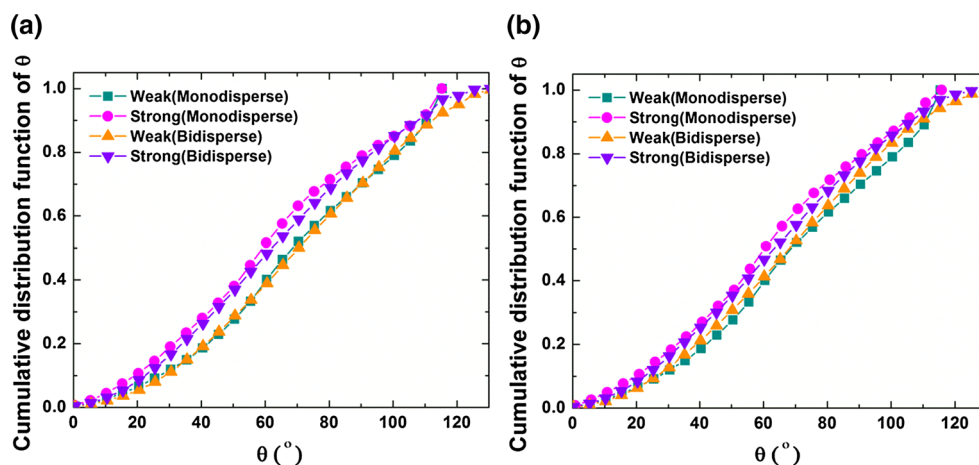


**Fig. 5** Cumulative distribution functions of  $\theta$ , where both  $\theta_1$  and  $\theta_2$  are treated as a single variable  $\theta$ , in the weak and strong networks for the monodisperse and bidisperse systems. **a** Pressure=0.001 MPa, **b** pressure=100 MPa

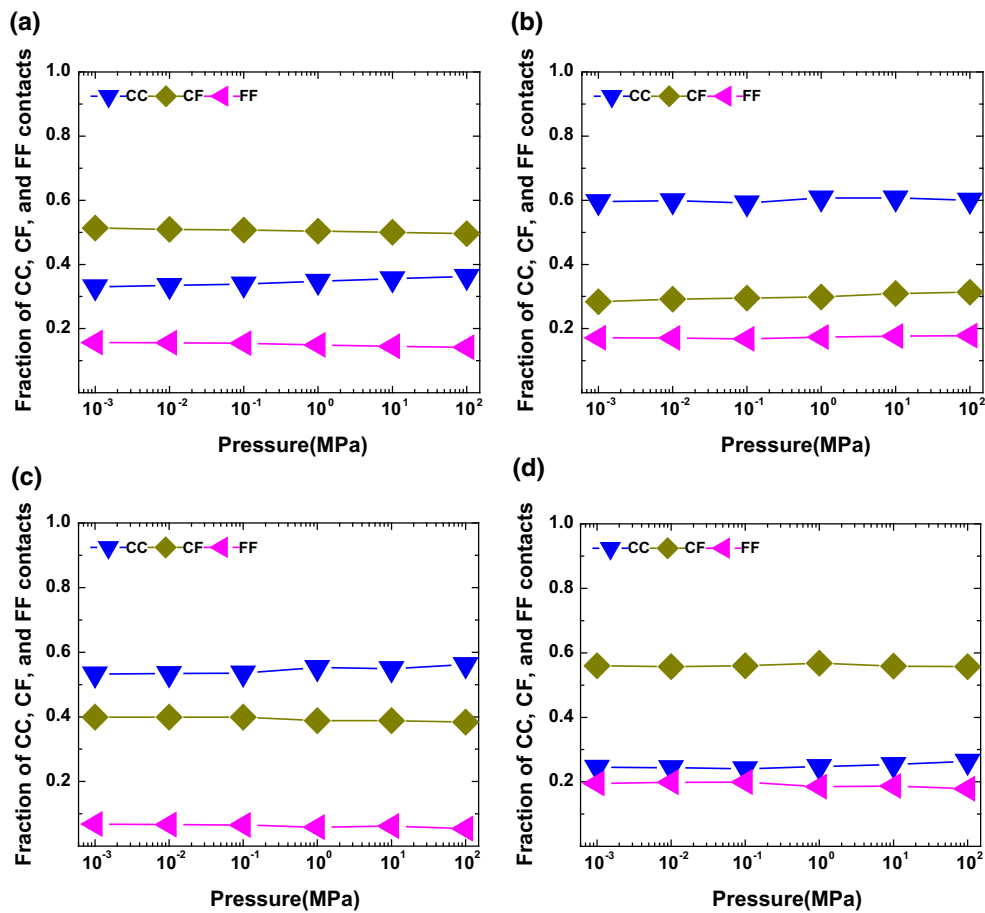


**Fig. 6** **a** Fraction of coarse-coarse (CC), coarse-fine (CF), and fine-fine (FF) contacts with respect to the total contacts as a function of pressure for bidisperse systems. **b** Fraction of CC, CF, and FF contacts

in the strong contact network. **c** Fraction of chainlike structures in the strong network. **d** Fraction of chainlike structures in the weak network

contacts is the CF contacts, which is in a strong contrast with the CC contacts dominating the strong contact network.

It should be pointed out that the previous 2-dimensional contact dynamic simulation results qualitatively indicate that the strong contact forces preferentially pass through the larger particles for the polydisperse system under simple shear load [42]. The contact dynamic simulations assume the particles are perfectly rigid, regardless of finite deformation of particles under pressures [15]. In contrast, the DEM simulations can take small level of particle deformation into account. The current 3-dimensional DEM simulations for the bidisperse systems under compression quantitatively indicate that CC contacts dominate the strong contact network, as well as the chainlike structures in the strong contact network. In contrast, CF contacts dominate the overall contact network, as well as the chainlike network in the weak contact network. Furthermore, it is worth mentioning that some of the theoretical analyses of force-chain length in literature usually assume that the probability of a particle (or force segment) involved in a force chain is a constant [38,39]. However,

the current simulation results indicate that this assumption is no longer appropriate for bidisperse systems, where the chainlike network prefers to pass through CC contacts in the strong network. However, the identification of the underlying mechanism of such higher probability of CC contacts in the chainlike structures deserves further investigation, and should be taken into account in a more advanced future model.

### 3.3 Response of contact orientation to the compressive load

The structure of contact force network is characterized by orientation distribution of contact vectors [43]. The angle  $\varphi$  is defined in the local spherical coordinate system as the angle between the contact vector and the vertical direction (parallel to the compressive direction). Therefore,  $\varphi = 0^\circ$  is a vertical contact and  $\varphi = 90^\circ$  is a horizontal contact. Figure 7 shows the distribution of angle  $\varphi$  as a function of pressure for both monodisperse and bidisperse simulation systems for two

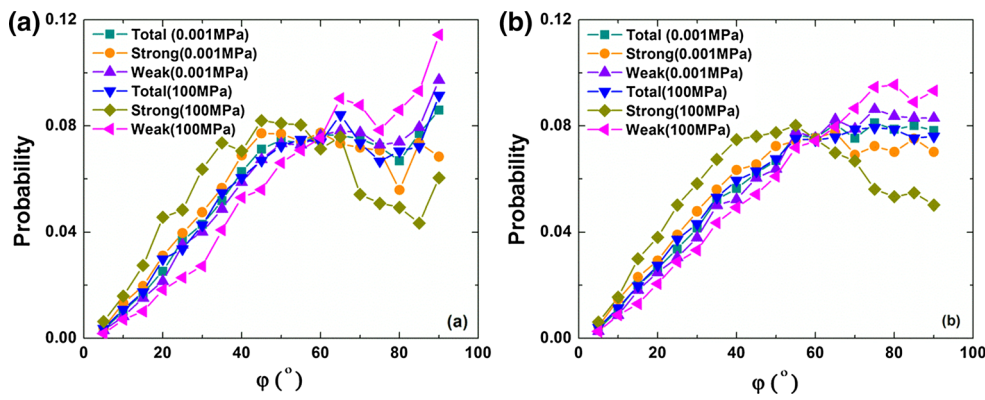


Fig. 7 Response of contact orientation in strong and weak networks to external load for both monodisperse and bidisperse systems

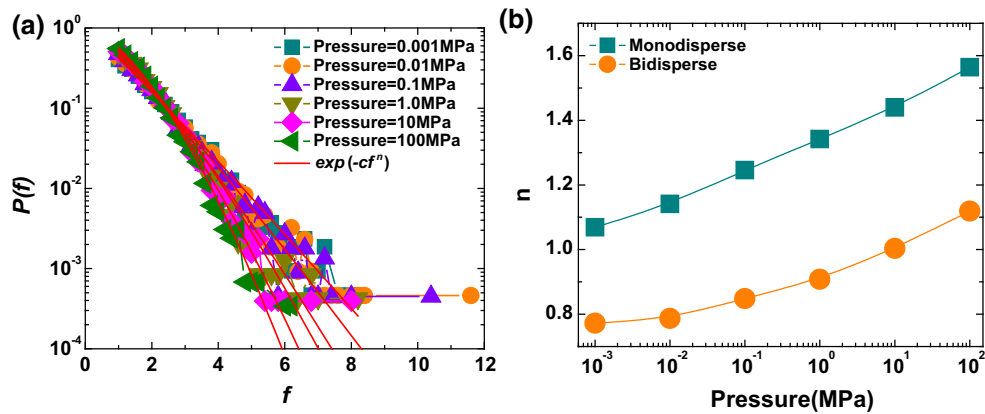


Fig. 8 Tails of probability distribution of the contact forces for monodisperse and bidisperse systems as a function of pressure

extreme loadings. One of the remarkable outcomes is that the strong and weak contact networks have completely different dynamic response to the external loads. With increasing pressure, the strong contact network develops a peak at around  $\phi$  of  $50^\circ$  for both monodisperse and bidisperse systems. In contrast, the distributions of contact orientation in the weak contact network develop a peak around  $\phi$  of  $90^\circ$  for both simulation systems. Moreover, the probabilities of distribution of contact orientations in the strong network increases for the contact orientation less than  $60^\circ$  and decreases for contact orientation greater than  $60^\circ$ , while the weak network exhibits the opposite trends. When the whole contact ensemble is considered, such opposite responses of strong and weak contact networks are swept away by the ensemble average and the total distribution of  $\phi$  for all the contacts is very similar for low and high pressure.

### 3.4 Contact force statistics and participation number

Different models have been proposed in the literature to describe the behavior of  $P(f)$ . For example, along with experimental data [2,25], the recent theoretical results and numerical simulations indicate that the force distribution

decays much faster than at an exponential rate, hence, it is doubtful that exponential decay is a generic property of jammed particles [7, 10, 27]. In this study, the following general equation proposed in [7, 27] is used to fit decay behavior of contact forces larger than the mean contact force for all the simulation systems:

$$P(f) = e^{-cf^n} \tag{5}$$

where  $c$  and  $n$  are fitting parameters. The best fitting values of  $n$  as a function of compressive loadings for monodisperse and bidisperse systems are investigated and shown in Fig. 8. Figure 8a presents results for monodisperse system for six different loadings to illustrate determination of  $n$  based on the regression analysis. Figure 8b presents values for  $n$  for all loadings and both monodisperse and bidisperse systems. It can be seen that the value of  $n$  increases with increasing compressive loading for both systems, indicating a more homogeneous force distribution as compressive force increases. Furthermore, the degree of homogeneity of contact force can also be quantified by the participation number  $\Gamma$  [3, 8]:



$$\Gamma = \frac{1}{M \sum_{i=1}^M q_i^2}, \quad q_i = f_j / \sum_{j=1}^M f_j \quad (6)$$

where the  $M$  is the number of total contacts and  $f_j$  is the magnitude of the  $j$ th contact force. From the definition of Eq. (6), the complete homogeneous distribution of contact force results in participation number of one. In contrast, the limit of complete localization corresponds to participation number of zero, i.e.,  $\Gamma \approx 0$ . Participation number is computed using Eq. (6) and results show that for monodisperse system the participation number increases from 0.51 to 0.65 with increase of pressure from 0.001 to 100 MPa. For bidisperse system, the participation number increases from 0.39 to 0.55 with increase of pressure from 0.001 to 100 MPa. These results indicate that contact forces are more localized at a lower pressure than that at a higher pressure for both monodisperse and bidisperse systems. In addition, contact forces are more localized in the monodisperse system than that in the bidisperse system at fixed pressure. Those conclusions are also consistent with statistical distribution of contact forces.

Figure 8b indicates that for fixed compressive loading, the value of  $n$  is larger for monodisperse systems than that of the bidisperse systems. It should be noted that a large number of simulation and experimental results regarding force distribution have been reported in the literature. Some of them have been done for uniform size distribution [23, 24, 29, 44] or small size variation [3, 5, 19, 20]. However, the others are performed using particles with continuous size distributions [15, 42]. Our results indicate that although force distributions for monodisperse systems are qualitatively similar with their equivalent bidisperse counterparts, there are quantitative differences between them. Therefore, the nature of particle size distribution should be taken into consideration in order to quantitatively compare different results.

## 4 Conclusions

Using DEM simulations, the properties of strong and weak force networks in jammed granular media under uniaxial compression are investigated. In particular, spatial correlation and distribution of contact angle, chainlike structures in the strong and weak force networks, response of force networks to the external load, and statistical analysis of contact forces is presented. The simulation results show that about 60% of contacts belonging to the strong network form the chainlike structures. In contrast, about 32–45% of contacts in the weak contact network are able to form the chainlike structures, increasing with increasing pressure. For the bidisperse systems, the total contact network is dominated by the coarse-fine particle contacts; however, coarse-coarse particle contacts dominate the strong contact network, as well as the chainlike structures. In the strong force network the proba-

bilities of contact orientation with respect to the compressive direction increases for the contact orientation less than  $60^\circ$  and decreases for the contact orientation greater than  $60^\circ$ , while the weak network exhibits the opposite trends. The statistical distribution of the strong contact forces can be depicted by  $P(f) = \exp(-cf^n)$  where the values of  $n$  increase with increasing pressure, indicating better homogeneity of contact forces, which is consistent with the analysis based on participation number.

This work provides the further insight about the properties of strong and weak contact networks within three dimensional jammed granular media. Those properties are vital for gaining a deeper understanding of the behavior of macroscopic jammed systems from particle scale information. Future work should target examination of the properties of force networks under the combination of shear and compression loads.

**Acknowledgements** The authors gratefully acknowledge partial financial support from the National Science Foundation (NSF) through Grants # EEC-0540855 and EEC-0951845.

## Compliance with ethical standards

**Conflict of interest** We declare that we do not have any commercial or associative interest that represents a conflict of interest in connection with the work submitted.

## References

- O'Hern, C.S., Silbert, L.E., Liu, A.J., Nagel, S.R.: Jamming at zero temperature and zero applied stress: the epitome of disorder. *Phys. Rev. E* **68**(1), 011306 (2003)
- Majmudar, T.S., Behringer, R.P.: Contact force measurements and stress-induced anisotropy in granular materials. *Nature* **435**(1079), 1079–1082 (2005)
- Makse, H.A., Johnson, D.L., Schwartz, L.M.: Packing of compressible granular materials. *Phys. Rev. Lett.* **84**(18), 4160–4163 (2000)
- Snoeijer, J.H., Vlugt, T.J.H., van Hecke, M., van Saarloos, W.: Force network ensemble: a new approach to static granular matter. *Phys. Rev. Lett.* **92**(5), 054302 (2004)
- Corwin, E.I., Jaeger, H.M., Nagel, S.R.: Structural signature of jamming in granular media. *Nature* **435**(7045), 1075–1078 (2005)
- O'Hern, C.S., Langer, S.A., Liu, A.J., Nagel, S.R.: Force distributions near jamming and glass transitions. *Phys. Rev. Lett.* **86**(1), 111–114 (2001)
- Wang, X., Zhu, H.P., Luding, S., Yu, A.B.: Regime transitions of granular flow in a shear cell: a micromechanical study. *Phys. Rev. E* **88**(3), 032203 (2013)
- Zhang, H.P., Makse, H.A.: Jamming transition in emulsions and granular materials. *Phys. Rev. E* **72**(1), 011301 (2005)
- Cates, M.E., Wittmer, J.P., Bouchaud, J.P., Claudin, P.: Jamming, force chains, and fragile matter. *Phys. Rev. Lett.* **81**(9), 1841–1844 (1998)
- Tighe, B.P., van Eerd, A.R.T., Vlugt, T.J.H.: Entropy maximization in the force network ensemble for granular solids. *Phys. Rev. Lett.* **100**(23), 238001 (2008)

11. Thornton, C.: Force transmission in granular media. *KONA Powder Part. J.* **15**, 81–90 (1997)
12. Owens, E.T., Daniels, K.E.: Sound propagation and force chains in granular materials. *EPL (Europhys. Lett.)* **94**(5), 54005 (2011)
13. Kondic, L., Goulet, A., Hern, C.S.O., Kramar, M., Mischaikow, K., Behringer, R.P.: Topology of force networks in compressed granular media. *EPL (Europhys. Lett.)* **97**(5), 54001 (2012)
14. Radjai, F., Wolf, D.E., Jean, M., Moreau, J.-J.: Bimodal character of stress transmission in granular packings. *Phys. Rev. Lett.* **80**(1), 61–64 (1998)
15. Radjai, F., Roux, S., Moreau, J.J.: Contact forces in a granular packing. *Chaos* **9**(3), 544–550 (1999)
16. Walker, D., Tordesillas, A., Thornton, C., Behringer, R., Zhang, J., Peters, J.: Percolating contact subnetworks on the edge of isostaticity. *Granul. Matter* **13**(3), 233–240 (2011)
17. Bi, D., Zhang, J., Chakraborty, B., Behringer, R.P.: Jamming by shear. *Nature* **480**(7377), 355–358 (2011)
18. Liu, C.-H., Nagel, S.R., Schecter, D.A., Coppersmith, S.N., Majumdar, S., Narayan, O., Witten, T.A.: Force fluctuations in bead packs. *Science* **269**(5223), 513–515 (1995)
19. Mueth, D.M., Jaeger, H.M., Nagel, S.R.: Force distribution in a granular medium. *Phys. Rev. E* **57**(3), 3164–3169 (1998)
20. Blair, D.L., Mueggenburg, N.W., Marshall, A.H., Jaeger, H.M., Nagel, S.R.: Force distributions in three-dimensional granular assemblies: effects of packing order and interparticle friction. *Phys. Rev. E* **63**(4), 041304 (2001)
21. Radjai, F., Jean, M., Moreau, J.-J., Roux, S.: Force distributions in dense two-dimensional granular systems. *Phys. Rev. Lett.* **77**(2), 274–277 (1996)
22. Landry, J.W., Grest, G.S., Silbert, L.E., Plimpton, S.J.: Confined granular packings: structure, stress, and forces. *Phys. Rev. E* **67**(4), 041303 (2003)
23. Silbert, L.E., Grest, G.S., Landry, J.W.: Statistics of the contact network in frictional and frictionless granular packings. *Phys. Rev. E* **66**(6), 061303 (2002)
24. Yang, R.Y., Zou, R.P., Yu, A.B., Choi, S.K.: Characterization of interparticle forces in the packing of cohesive fine particles. *Phys. Rev. E* **78**(3), 031302 (2008)
25. Zhou, J., Long, S., Wang, Q., Dinsmore, A.D.: Measurement of forces inside a three-dimensional pile of frictionless droplets. *Science* **312**(5780), 1631–1633 (2006)
26. O’Hern, C.S., Langer, S.A., Liu, A.J., Nagel, S.R.: Random packings of frictionless particles. *Phys. Rev. Lett.* **88**(7), 075507 (2002)
27. van Eerd, A.R.T., Ellenbroek, W.G., van Hecke, M., Snoeijer, J.H., Vlugt, T.J.H.: Tail of the contact force distribution in static granular materials. *Phys. Rev. E* **75**(6), 060302 (2007)
28. Coppersmith, S.N., Liu, C.-H., Majumdar, S., Narayan, O., Witten, T.A.: Model for force fluctuations in bead packs. *Phys. Rev. E* **53**(5), 4673–4685 (1996)
29. Ngan, A.H.W.: Mechanical analog of temperature for the description of force distribution in static granular packings. *Phys. Rev. E* **68**(1), 011301 (2003)
30. Radjai, F., Wolf, D.E.: Features of static pressure in dense granular media. *Granul. Matter* **1**(1), 3–8 (1998)
31. Rycroft, C.H., Orpe, A.V., Kudrolli, A.: Physical test of a particle simulation model in a sheared granular system. *Phys. Rev. E* **80**(3), 031305 (2009)
32. Mindlin, R.D.: Compliance of elastic bodies in contact. *J. Appl. Mech.* **16**, 259–268 (1949)
33. Johnson, K.L., Johnson, K.L.: *Contact Mechanics*. Cambridge University Press, Cambridge (1987)
34. Tsuji, Y., Tanaka, T., Ishida, T.: Lagrangian numerical simulation of plug flow of cohesionless particles in a horizontal pipe. *Powder Technol.* **71**(3), 239–250 (1992)
35. Deng, X., Scicolone, J.V., Davé, R.N.: Discrete element method simulation of cohesive particles mixing under magnetically assisted impaction. *Powder Technol.* **243**, 96–109 (2013)
36. Arévalo, R., Zuriguel, I., Maza, D.: Topology of the force network in the jamming transition of an isotropically compressed granular packing. *Phys. Rev. E* **81**(4), 041302 (2010)
37. Peters, J.F., Muthuswamy, M., Wibowo, J., Tordesillas, A.: Characterization of force chains in granular material. *Phys. Rev. E* **72**(4), 041307 (2005)
38. Desmond, K.W., Young, P.J., Chen, D., Weeks, E.R.: Experimental study of forces between quasi-two-dimensional emulsion droplets near jamming. *Soft Matter* **9**(12), 3424–3436 (2013)
39. Zhang, L., Wang, Y., Zhang, J.: Force-chain distributions in granular systems. *Phys. Rev. E* **89**(1), 012203 (2014)
40. Jose, J., van Blaaderen, A., Imhof, A.: Random three-dimensional jammed packings of elastic shells acting as force sensors. *Phys. Rev. E* **93**(6), 062901 (2016)
41. Tordesillas, A., Walker, D.M., Froyland, G., Zhang, J., Behringer, R.P.: Transition dynamics and magic-number-like behavior of frictional granular clusters. *Phys. Rev. E* **86**(1), 011306 (2012)
42. Voivret, C., Radjai, F., Delenne, J.Y., El Youssoufi, M.S.: Multiscale force networks in highly polydisperse granular media. *Phys. Rev. Lett.* **102**(17), 178001 (2009)
43. Deng, X., Davé, R.: Dynamic simulation of particle packing influenced by size, aspect ratio and surface energy. *Granul. Matter* **15**(4), 401–415 (2013)
44. Antony, S.J.: Evolution of force distribution in three-dimensional granular media. *Phys. Rev. E* **63**(1), 011302 (2000)